Silicon (2022) 14:12665–12674
https://doi.org/10.1007/s12633-022-01982-3

ORIGINAL PAPER

A Highly Sensitive Photonic Crystal Fiber Gas Sensor for the Detection of Sulfur Dioxide

Elizabeth Caroline Britto[1] · S. Mohamed Nizar[1] · Prabu Krishnan[2]

Received: 14 March 2022 / Accepted: 12 June 2022 / Published online: 23 June 2022

Abstract
Sulfur dioxide (SO_2) is one of the most prevalent contaminants in the atmosphere. It is mostly generated as a byproduct of the burning of sulfur-containing coal and oils, as well as the smelting of various ores. SO_2 contributes to the development of major diseases such as asthma and chronic bronchitis. In this paper, we proposed a Wheel Structured circular air hole Photonic Crystal Fiber (WS-PCF) based gas sensor to detect SO_2 gas. The proposed WS-PCF gas sensor consists of a four-layer-thick circular cladding air hole. The diameter of the first layer varies throughout the optimization procedure, while the diameters of the succeeding three layers remain constant. The numerical investigation on the sensor parameters such as numerical aperture, effective area, non-linearity, confinement, loss and the relative sensitivity of the proposed sensor are extensively analyzed in a wavelength range of 0.9 µm to 1.2 µm. The proposed WS-PCF gas sensor offers the highest relative sensitivity of 83.64% and a lower confinement loss of $6.34 \times 10^{-9} dB/km$. The proposed sensor is simple and offers 14% high sensitivity and very low confinement loss (10^{-3} reported in literature) compared with the exist literature.

Keywords WS-PCF gas sensor · Circular cladding · Relative sensitivity · Confinement loss · Non-linearity and numerical aperture

1 Introduction

Technical advancements in detecting gas concentration and composition, such as Volatile Organic Compounds (VOC), are urgently needed for the early detection of gas leaks and explosions as industrial automation and artificial intelligence increase [1–3]. Gas sensors use electro-chemistry, contact combustion, optical spectroscopy, chemical absorption, and other mechanisms to work [4–6]. Optical signals travel through the optical fiber and respond to the environment in the detection zone, which is made up of different fiber configurations. The optical fiber's characteristics make it a suitable candidate for constructing high-performance gas sensors in recent years [7–9]. The interference and resonance enhancement in various unique fiber topologies significantly enhanced the optical fiber gas sensor's sensitivity [10, 11].

Due to its high sensitivity, small size, and flexibility, the PCF-based sensor is precious. The characteristics can be determined by optimizing the size, shape, and position of the core and cladding, as well as by varying the pitch calibration. In PCF sensors excellent optical properties are achieved due to the distribution of holes. Moreover, there is a scope of tuning the optical property of the PCF sensor by altering the arrangement, size and shape of the holes. These parameters are difficult to achieve with conventional optical fiber [12–14].

PCF is resistant to the external environment, it measures minute temperature variations quickly, and it can also detect various gases and chemicals that are harmful to humans. Different sensors are used for the detection of different parameters. The PCF based SPR sensor concurrently measures RI, magnetic field and temperature [15] and SPR sensor which detects liver tissue [16]. The PCF is used in a variety of sensing applications, including temperature, bio-sensing, gas sensing, and temperature sensing [17–25]. The presence of

✉ S. Mohamed Nizar
nizar.shabu@gmail.com

Elizabeth Caroline Britto
carolinebritto96@gmail.com

Prabu Krishnan
prabuk@nitk.edu.in

[1] Department of Electronics and Communication Engineering, IFET College of Engineering, Villupuram, Tamilnadu, India

[2] Department of Electronics and Communication Engineering, National Institute of Technology Karnataka, Surathkal, India

air holes in a PCF cladding enables both direct light transmission and the introduction of analytes (gases, chemicals, etc.) into the air holes, resulting in constrained light interaction with the sample and the development of novel sensing applications [26].

The main objective of this paper is to demonstrate the detection of SO_2 at a temperature of 25 °C. SO_2 is a colorless, flammable, reactive gas with a pungent odour. It is produced in a variety of natural and human-made ways. SO_2 emissions are primarily caused by the combustion of high-sulfur coal and heating oil in power plants, followed by industrial boilers and metal smelting [27]. When asthmatic children and adults exercise outdoors, SO_2 can temporarily impair breathing. Short-term exposure of asthmatic individuals to elevated SO_2 levels while moderately exercising may result in diminished lung function, which may manifest as wheezing, chest tightness, or shortness of breath [28].

In this paper a high sensitivity WS-PCF sensor is proposed for SO_2 gas detection compared with existing methods. To sense the SO_2 gas, light confinement occurs in the area of the core at wavelengths ranging from 0.9 µm to 1.3 µm. The performance of the WS-PCF gas sensor is simulated by COMSOL Multiphysics software and analysis are carried for different sensing parameters. The sequence of the manuscript is as follows: sensor design, numerical analysis, results and discussion, and conclusion.

2 Proposed Gas Sensor Design

Figure 1 illustrates the cross-section view of the proposed WS-PCF gas sensor. The design incorporates a circular core surrounded by four layers of cladding. The diameter of the third, fifth, ninth, and eleventh air holes in the first cladding layer is 1.26 µm. The cladding has 12 air holes in each of the four layers. The diameter of second cladding layer is 0.635 µm. The diameter of third and fourth cladding layers has a diameter of 0.705 µm. The core is located in the centre, where light confinement occurs, and measures 1.27 µm in diameter. The WS-PCF gas sensor's sensing capability is determined by several critical parameters, one of which is the pitch. Pitch is the distance between center to center air hole and is represented as Λ. The design maintains a 2 µm pitch. The performance of the gas sensor is investigated by varying the diameter of the 3rd, 5th, 9th, and 11th cladding air holes. Silica is used as a background material because it is more efficient than other materials due to its 1.45 Refractive Index (RI). The core is filled with SO_2 gas having a RI of 1.3396, while the cladding is filled with air having a RI of 1. The Perfectly Matched Layer (PML) that surrounds the gas sensor design prevents light from scattering. The proposed WS-PCF gas sensor has a PML of 0.8 µm.

The gas is sensed in the hollow core of the PCF gas sensor. The RI of the gas to be sensed is placed in the core, where light and the gas samples overlaps with each other. When the gas is passed to the core of the hollow core of the PCF gas sensor there is a deviation at the output of the sensor and it is measured by Beer-Lambert law. The deviated output gives the sensitivity of the gas to be sensed.

Various factors are studied, including sensitivity, confinement loss, effective refractive index (n_{eff}), effective mode area (A_{eff}), non-linearity, and numerical aperture (NA). Due to the difficulty associated with fabrication, the proposed WS-PCF gas sensor's core and cladding are circular. Numerous fabrication methods are available. Among the most prevalent are drilling, die-casting, stack and draw, and sol–gel fabrication. However, only a few of these fabrication procedures offer exceptional outcomes. Stack and draw will produce superior results during the circular air hole construction process. However, the disadvantage of this process is that if the design is intricate, the final production may deviate from the original. To address this issue, a sol–gel manufacturing process is used to construct this WS-PCF gas sensor efficiently.

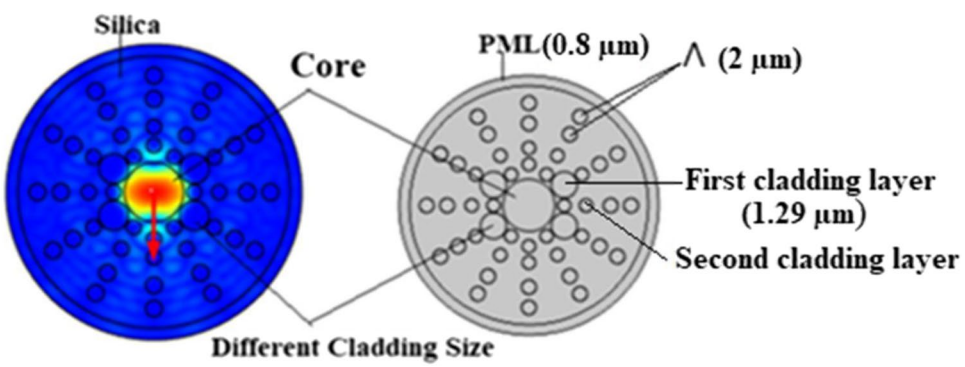

Fig. 1 Structure of WS-PCF gas sensor

Table 1 Sensitivity for different cladding diameter for the wavelength of 0.8 µm to 1.3 µm

Sensitivity (%)				
λ (µm)	1.26 µm	1.27 µm	1.28 µm	1.29 µm
0.8	83.733	63.497	35.427	66.81
0.9	23.799	25.829	31.656	34.195
1	51.785	45.538	43.809	41.635
1.1	62.65	62.785	62.992	62.496
1.2	82.676	83.057	83.377	83.646
1.3	66.553	76.333	81.045	82.791

3 Mathematical Equations

Due to the limited number of air holes, optical power radiates from the core and leaks into the cladding region, resulting in confinement loss. The wavelength and imaginary part of the n_{eff} affect confinement loss, which can be calculated as [29]

$$L_c = 8.686 k_0 x I_m\left(n_{eff}\right) x 10^6 \tag{1}$$

$$k_0 = \frac{2\pi}{\lambda}$$

where L_c is the confinement loss, k_0 is the free space wave number, and $I_m\left(n_{eff}\right)$ is the N_{eff}'s imaginary part. Beer-Lambert law is used to calculate the deviation in light intensity, as light and gas elements interrelate in the core. The mathematical formula is given as [30]

$$I(\lambda) = I_0(\lambda)\exp\left(-r\theta_m LC\right) Wm^{-2} \tag{2}$$

where $I(\lambda)$ and $I_0(\lambda)$ Represent the amplitudes of light signal with and without gas samples, respectively. r is the relative sensitivity, θ_m is the absorption coefficient, L is the fiber length, C is the gas concentration, and λ is the SO_2 absorption wavelength.

The phenomenon of shared action between the gas components and guiding light at an exact wavelength is relative sensitivity. The Beer-Lambert law states that relative sensitivity varies with gas attention and wavelength, which can be calculated as [31]

$$r = \frac{n_r}{n_{eff}} Xf \tag{3}$$

where n_r denotes SO_2's RI, n_{eff} denotes SO_2's modal effective RI, and f denotes frequency of relative sensitivity. Furthermore, the coefficient is defined as the ratio of optical power in core to the total power of device, which is calculated as [32]

$$\mathrm{f} = \frac{\int_{\mathrm{Sample}} \mathrm{Re}(\mathrm{E_x H_y} - \mathrm{E_y H_x})\mathrm{dxdy}}{\int_{\mathrm{total}} \mathrm{Re}(\mathrm{E_x H_y} - \mathrm{E_y H_x})\mathrm{dxdy}} \times 100 \tag{4}$$

E_x and E_y are the electric fields of x and y elements, and H_x and H_y are the magnetic fields of x and y fundamentals.

During optical power propagation through the core, light concentrates on a precise area that differs from the geometrical size of the core and this area is known as the A_{eff}. It can be calculated using Eq. (5) given in [33]

$$A_{eff} = \frac{(\iint |E|^2 dxdy)^2}{\iint |E|^4 dxdy} \mu m^2 \tag{5}$$

where A_{eff} is the effective area of the core and E denotes the guided mode's transverse electric fields. Other parameters considered for the fiber optic gas sensor design is nonlinearity. The higher nonlinearity-based PCF value is used for signal processing. Non-linearity is inversely proportional

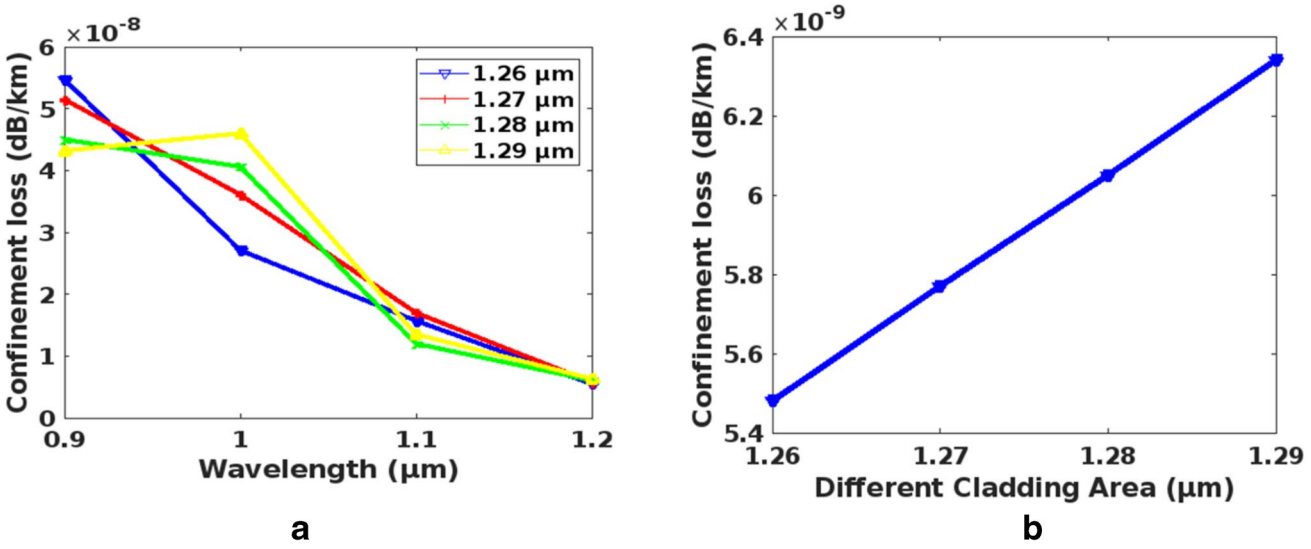

Fig. 2 (**a**) the confinement loss versus wavelength for various core diameters, (**b**) Relationship between confinement loss and cladding diameter

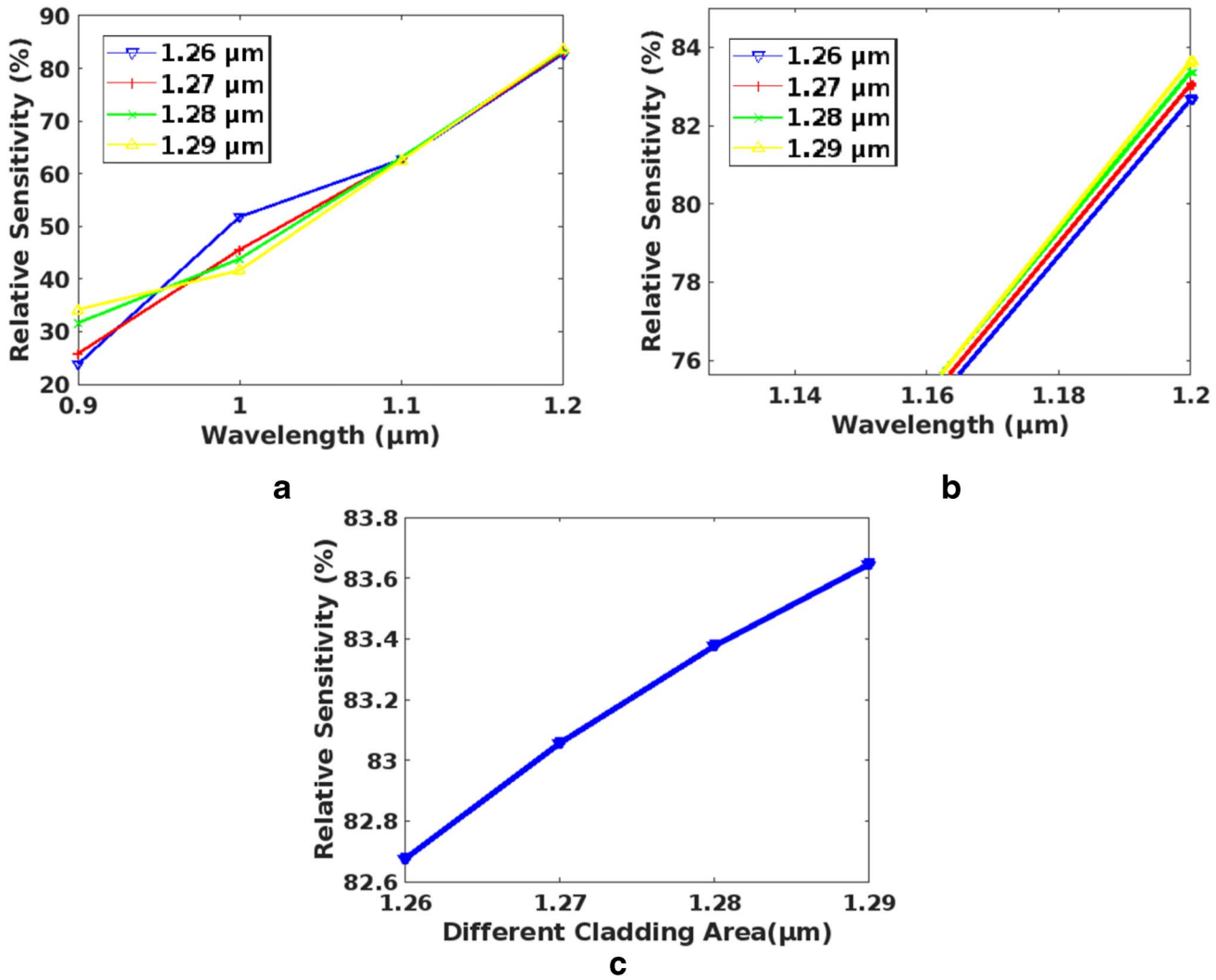

Fig. 3 (**a**) Variation in relative sensitivity as a function of air hole diameter in the cladding. (**b**) Enlarged view of sensitivity graph and (**c**). The relative sensitivity vs the cladding air hole diameter at 1.2 μm wavelength

to the A_{eff} of the core, which can be calculated using the equation [34].

$$Y(\lambda) = \frac{2\pi * n_2}{\lambda * A_{eff}} \mathrm{W}^{-1} m^{-1} \tag{6}$$

The non-linear co-efficient of silica material is represented as n_2.

The light gathering capacity of the fiber is calculated by Numerical Aperture (NA), as given by the following equation.

$$NA = \frac{1}{\sqrt{1 + \frac{\pi \mathrm{x} A_{\mathrm{eff}}}{\lambda^2}}} \tag{7}$$

The concentration of the SO_2 gas can find by using the following formula

$$\mathrm{n} = 1 + \frac{\alpha \mathrm{x} \rho}{2} \tag{8}$$

where, α is molecule palarizability and its value is 3.882. ρ is number of molecules per unit volume.

4 Numerical Analysis and Discussions

To detect SO_2, a WS-PCF gas sensor is used, and the diameter of the cladding air holes is varied. The diameters of the third, fifth, ninth, and eleventh air holes in the first cladding layer are analyzed. The values of different diameters are 1.26 μm, 1.27 μm, 1.28 μm, and 1.29 μm. Sensing parameters like sensitivity, A_{eff}, confinement loss, non-linearity and numerical aperture are analyzed for different cladding diameters of 1.26 μm, 1.27 μm, 1.28 μm, and 1.29 μm. For

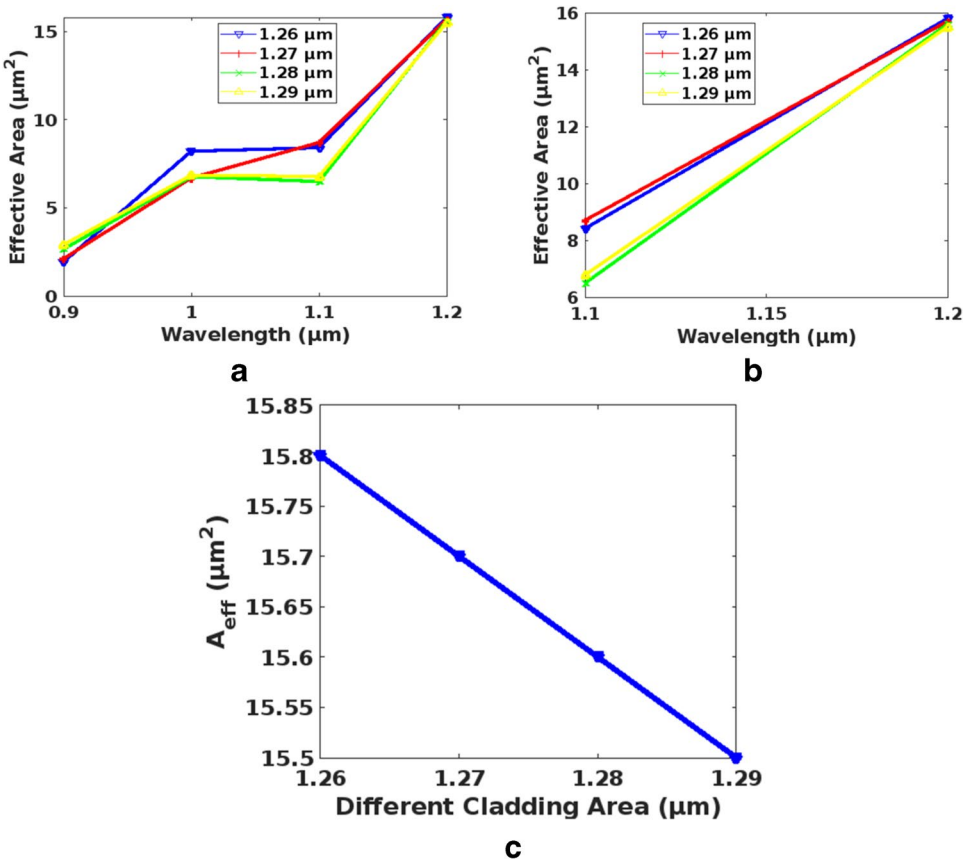

Fig. 4 (**a**) Variation in the A_{eff} of four cladding diameter with respect to wavelength (**b**). Enlarged graph of A_{eff} (**c**). A_{eff} vs. different cladding diameter at 1.2 μm wavelength

the purpose of optimize the wavelength values from 0.8 μm to 1.3 μm are analyzed and it is tabulated in Table 1.

From Table 1 the sensitivity for all the four different cladding diameters are linearly increasing for the wavelength between 0.9 μm and 1.2 μm. Above and below these wavelength ranges the sensitivity is not linear. As the size of the first cladding layer increases, the sensitivity increases. At 1.29 μm of the first layer cladding layer diameter the

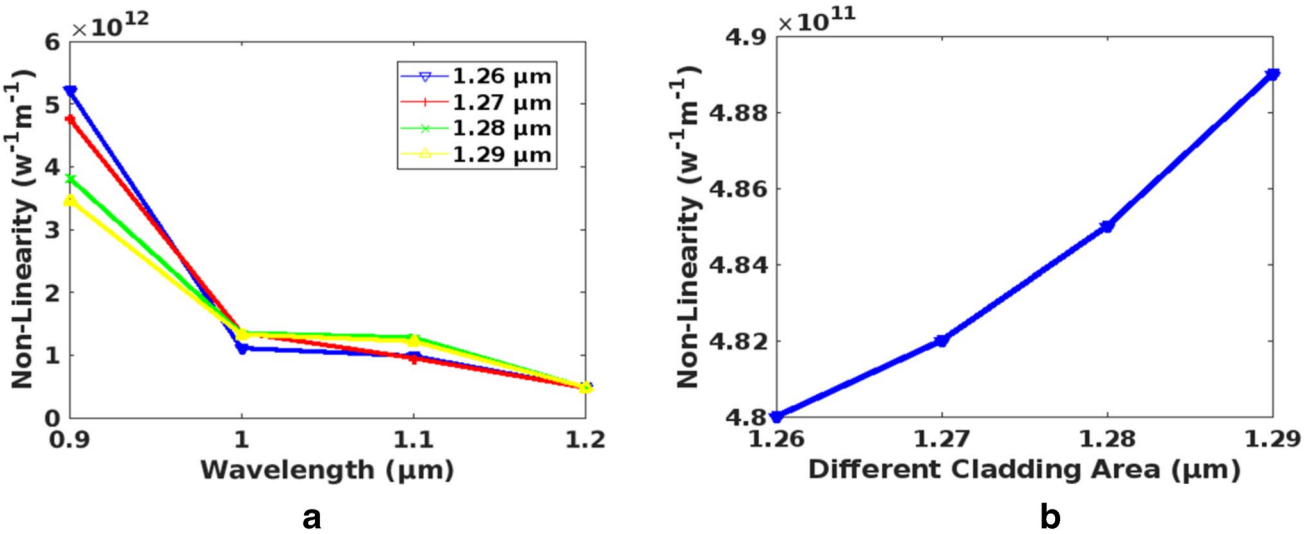

Fig. 5 (**a**) Non-linearity variation with respect to wavelength and (**b**) Graph between non-linearity vs different cladding diameter at 1.2 μm wavelength

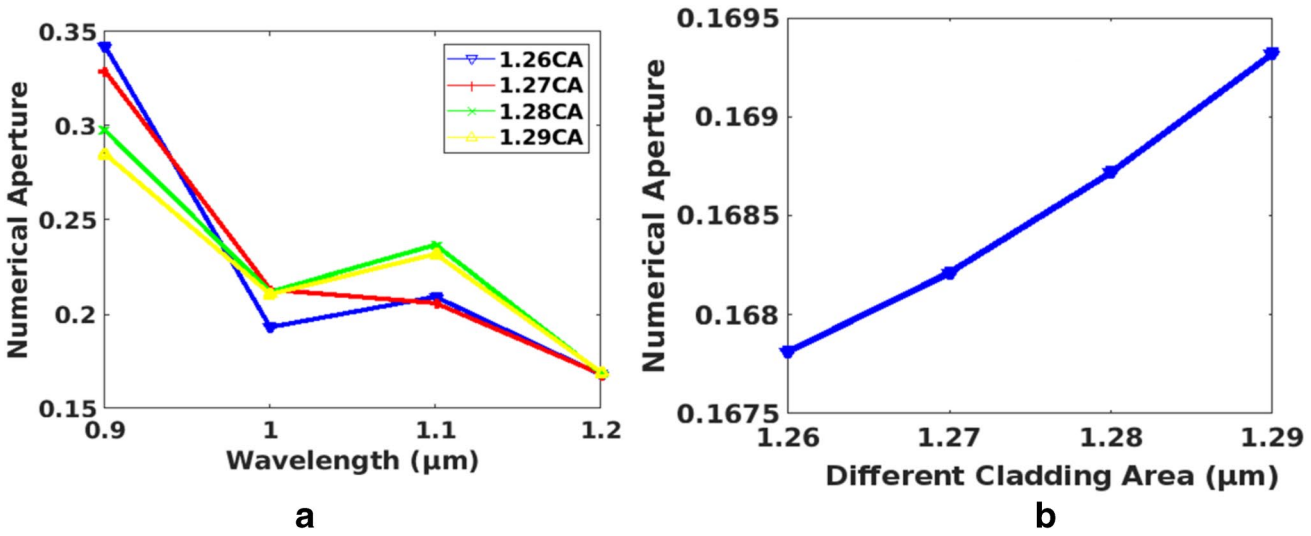

Fig. 6 (**a**) NA vs wavelength for different first layer cladding diameter and (**b**) Graph between NA and different cladding diameter at 1.2 μm wavelength

best sensitivity of 83.64% is achieved for the wavelength of 1.2 μm.

The confinement loss or loss curve is explained through Eq. (1). Figure 2(a) illustrates the loss curves for various cladding diameters in relation to wavelength, while Fig. 2(b) illustrates the loss curves in relation to cladding diameter for wavelengths ranging from 0.9 μm to 1.2 μm. The core area's light confinement is superior because the confinement loss is less as the wavelength propagates. In comparison, as the diameter of the cladding in the first layer increases, the confinement loss increases from 4.32×10^{-8} to 6.34×10^{-9} dB/km. This increase in confinement loss will have no effect on the PCF gas sensor's performance.

The proposed WS-PCF gas sensor is demonstrated in the gas sensing application. The sensible response depends mainly on the wavelength because the light-mater interaction is not the same for all-optical wavelengths. In Fig. 3(a), for different first layer cladding values of 1.26 μm, 1.27 μm, 1.28 μm, and 1.29 μm the sensitivity is plotted against the wavelength. The sensitivity is increased as wavelength increases. It means higher the optical wavelength and stronger the light-mater interaction. Figure 3(b) is the enlarged view of the sensitivity graph. In Fig. 3(c), the graph is drawn for the sensitivity w.r.t different cladding diameter. It is clearly shown that as the size of the cladding diameter increases, the sensitivity of WS-PCF gas sensor is increased due to more light is confined in the core region. The sensitivity of 1.29 μm cladding diameter compares high in the other three cladding diameters. The sensitivity of 1.26 μm cladding diameter is 82.676%, and the large cladding area of 1.29 μm is 83.646%.

Light confinement in a particular core area for a specific wavelength is called as A_{eff}. The A_{eff} increases linearly with wavelength for all cladding diameters this is due to the leakage of modes through the air holes. The graphs in Figs. 4(a) and 4(b) illustrate the A_{eff} in relation to the wavelength and the enlarged A_{eff}, respectively. It is understood that as the diameter of the cladding increases, the A_{eff} decreases, as illustrated in Fig. 4(c). A low A_{eff} of 0.155 μm^2 is achieved for first layer cladding diameter of 1.29 μm.

Non-linearity is a critical parameter in signal processing; a small effective area indicates a high power density is required for non-linear effects to be significant [35]. For optimal signal processing, the nonlinearity should be high. The nonlinearity for various cladding diameters is illustrated in Fig. 5(a). It is discovered that non-linearity decreases with increasing wavelength. Figure 5(b) Illustrates the non-linearity graph for various cladding diameters; as the cladding diameter increases, the non-linearity increases because the nonlinearity and A_{eff} are inversely proportional to each other. As a result, the proposed WS-PCF gas sensor is an attractive candidate for nonlinearity. It is concluded that signal processing in this PCF gas sensor is more efficient at large cladding diameters.

The NA graphs for various cladding areas are shown in Figs. 6 (a) and 6 (b). The NA decreases slightly with increasing frequency due to an increase in the difference in effective mode indices between cladding and core.

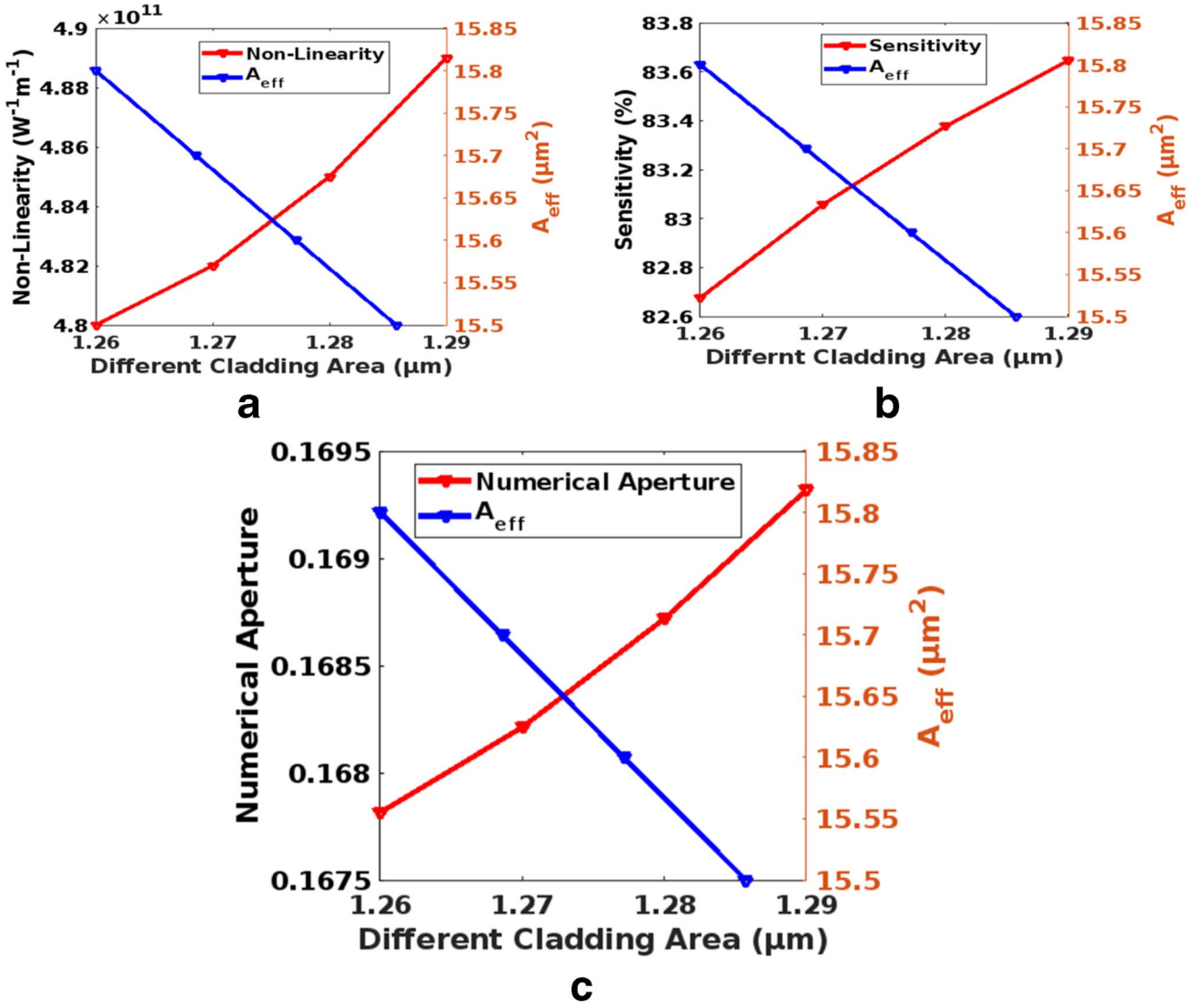

Fig. 7 (**a**) Cladding diameter dependence of non-linearity and A_{eff} for proposed WS-PCF gas sensor, (**b**) Cladding diameter dependence of sensitivity and A_{eff} and (**c**) Cladding diameter dependence of N.A and A_{eff}

From the Fig. 6, it is inferred as the size of the cladding diameter increases then there is a small increase in the numerical aperture at 1.2 μm wavelength this is due to the property of the N.A, were the light observing capacity is increased as the size of the cladding increased, The A_{eff} is a quantitative measure of the transverse area that covers a waveguide or fiber mode. The sensitivity, non-linearity, and numerical aperture for four different first layer cladding diameters of 1.26 μm, 1.27 μm, 1.28 μm, and 1.29 μm are compared with the A_{eff}. The four different cladding areas are 1.26 μm, 1.27 μm, 1.28 μm, and 1.29 μm; it is shown in Fig. 7. Further, the analysis is carried out to verify the relationship between non-linearity, mode area, sensitivity and N.A for different cladding diameter.

Figure 7(a) Illustrates, the effect of the diameter of the air hole in the first layer cladding on the mode area and relative sensitivity. Increases in the diameter of the first cladding air holes result in an increase in light confinement in the core region, this is due to more light is confine in the core region. As a result of the strong interaction between light and gas passing through the air hole, the A_{eff} through the core region is reduced, while the relative sensitivity of the SO_2 gas sensor is increased. Due to the inverse relationship between nonlinearity and A_{eff}, nonlinearity increases as cladding diameter increases, while mode area decreases in relation to cladding diameter, as illustrated in Fig. 7(b). As illustrated in Fig. 7(c), as the diameter of the cladding increases, the A_{eff} decreases, allowing for an increase in light

Table 2 Different concentrations of SO_2 gas

S.No	Concentration of SO_2 gas (PPM)	Refractive index	Sensitivity (%)
1	174,600	1.3388	81.919
2	174,700	1.3390	82.379
3	174,800	1.3392	82.824
4	174,900	1.3394	83.248
5	175,000	1.3396	83.646
6	175,100	1.3398	84.018
7	175,200	1.3400	84.363
8	175,300	1.3402	84.681
9	175,400	1.3404	84.974
10	175,500	1.3406	85.244

From the Table 2 it is understood that, as the concentration of SO_2 gas is increased, the RI and sensitivity of WS-PCF gas sensor is increases. Based on the concentration of the SO_2 gas the sensitivity varies, it means that the concentration of SO_2 and sensitivity are mutually proportional to each other (Fig. 8).

Table 3 compares the WS-PCF gas sensor to various structures for sensing different gases. The proposed WS-PCF gas sensor gives the best sensitivity and confinement loss of 83.646% and 6.34×10^{-09} dB/km respectively at 1.2 µm wavelength. By adjusting the diameter of the first layer cladding air hole, a maximum sensitivity of 83.646% is obtained, which is extremely high for the detection of SO_2 gas in comparison with V-PCF, H-PCF and micro-cored photonic PCF sensor [40, 41].

Table 3 Comparison of the proposed WS-PCF gas sensor with other PCF sensors

S.No	PCF Sensor	Sensitivity (%)	Confinement loss
1	HPC-PCF [36]	21.2	0.000025 dB/m
2	C-PCF [37]	72.04	—
3	Q-PCF [38]	64.69	4.38×10^{-06} dB/km
4	Triangular-PCF [39]	75.14	1.41×10^{-02} dB/m
5	H-PCF for sensing SO_2 [40]	58.34	8.94×10^{-04} dB/m
	V-PCF for sensing SO_2 [40]	59.34	5.93×10^{-04} dB/m
6	Micro-cored photonic crystal fiber for sensing SO_2 [41]	70	0.000136525 dB/m
7	Microstructure based gas sensor for ammonia detection [42]	70.25	1.202×10^{-1} dB/m
8	Proposed WS-PCF at 1.29 µm for sensing SO_2	83.646	6.34×10^{-09} dB/m

gathering capacity; as light gathering capacity increases, the NA increases as well. These analyses indicate that the WS-PCF sensor as designed is well suited for gas sensing applications. The RI and sensitivity of SO_2 gas is calculated using the Eq. (8) and the corresponding values are tabulated in Table 2.

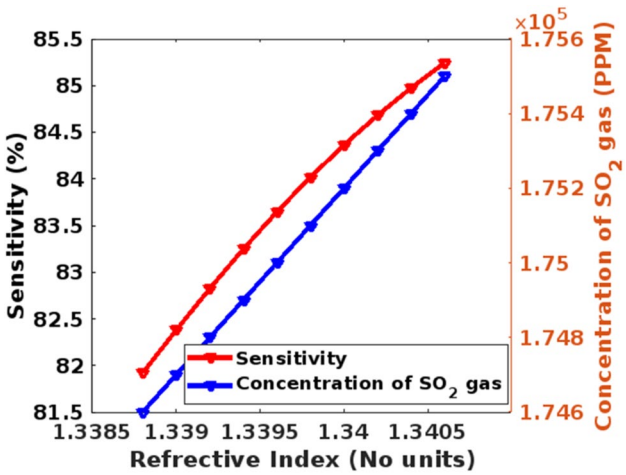

Fig. 8 Sensitivity depends on RI and concentration of SO_2 gas

5 Conclusion

This paper aims to improve the relative sensitivity of the proposed sensor for sensing SO_2 gas while reducing the fabrication complexity. It investigates the performance of the proposed WS-PCF gas sensor by increasing first layer cladding diameter. The different cladding diameters are 1.26 µm, 1.27 µm, 1.28 µm, and 1.29 µm. High sensitivity and confinement, loss of 83.646% and 6.34×10^{-09} dB/km respectively, is achieved for 1.29 µm diameter, and it is best compared with the previous methods. The combustion of fossil fuels transports SO_2, and it is a naturally occurring byproduct of volcanic eruptions. SO_2 causes severe issues to the human, especially in the respiratory tract. The proposed structure is easy to fabricate due to its simple design. The proposed WS-PCF gas sensor can detect colorless gas, and it is used as a biosensor.

Acknowledgements This research did not receive any specific grant from funding agencies in the public, commercial, or not-for-profit sectors.

Author Contributions All authors contributed to the study conception and design. Material preparation, data collection and analysis were performed by Dr. B. Elizabeth Caroline, Mr. S. Mohamed Nizar and

Dr. Prabu Krishnan. The first draft of the manuscript was written by Mr. S.Mohamed Nizar and all authors commented on previous versions of the manuscript. All authors read and approved the final manuscript.

Funding The authors declare that no funds, grants, or other support was received during the preparation of this manuscript.

Data Availability Data and materials are associated with the manuscript.

Declarations

Ethics Approval Yes.

Consent to Participate All the authors in this investigation voluntarily agree to participate in this research study.

Consent for Publication All authors provide consent for publication.

Competing Interests There are no competing interests.

Conflict of Interest There are no conflicts of interests.

Research Involving Human Participants and/or Animals Not Applicable.

Informed Consent Not Applicable.

References

1. Yamazoe N (2005) Toward innovations of gas sensor technology. Sens Actuators B 108:2–14
2. Yamazoe N, Shimanoe K (2009) New perspectives of gas sensor technology. Sens Actuat B 138:100–107
3. Schurmann G, Schafer K, Jahn C, Hoffmann H, Bauerfeind M, Fleuti E, Rappengluck B (2007) The impact of NOx, CO and VOC emissions on the air quality of Zurich airport. Atmos Environ 41(1):103–118
4. Toniolo R, Bortolomeazzi R, Svigelj R, Dossi N, Casella IG, Bragato C et al (2017) Use of an electrochemical room temperature ionic liquid-based microprobe for measurements in gaseous atmospheres. Sens Actuat B 240:239–247
5. Gao D, Zhang C, Wang S, Yuan Z, Wang S (2008) Catalytic activity of Pd/Al2O3 toward the combustion of methane. Catal Commun 9:2583–2587
6. Park HJ, Kim J, Choi NJ, Song H, Lee DS (2016) Nonstoichiometric Co-rich ZnCo2O4 hollow nanospheres for high performance formaldehyde detection at ppb levels. ACS Appl Mater Interfaces 8:3233–3240
7. Mohebati A, King TA (1988) Remote detection of gases by diode laser spectroscopy. J Mod Opt 35:319–324
8. Castrellon J, Paez G, Strojnik M (2002) Remote temperature sensor employing erbiumdoped silica fiber. Infrared Phys Technol 43:219–222
9. Sabri N, Aljunid SA, Salim MS, Ahmad RB, Kamaruddin R (2013) Toward optical sensors: review and applications. J Phys Conf Ser 423:012064
10. Dub´e WP, Brown SS, Osthoff HD, Nunley MR, Ciciora SJ, Paris MW, et al. (200+) Aircraft instrument for simultaneous, in situ measurement of NO3 and N2O5 via pulsed cavity ring-down spectroscopy. Rev Sci Instrum 77: 034101
11. Silva S, Frazao O (2018) Ring-down technique using fiber-based linear cavity for remote sensing. IEEE Sensors Lett 2:1–4
12. Cerqueria SA (2010) Recent progress and noval applications of photonic crystal fibers. Rep prog Phys 73:024401
13. Buczynski R (2004) Photonic crystal fibers. Acta Phys Pol A 106:141–167
14. Sharma, Anuj K, Pandey Ak, Kaur B (2018) A review of advancements (2007–2017) in plasmonics-based optical fiber sensors. Optical Fiber Technology 43: 20–34
15. Jing J, Liu K, Jiang J, Xu T, Wang S, Ma J, ... & Liu T (2022) Performance improvement approaches for optical fiber SPR sensors and their sensing applications. Photonics Research, 10(1), 126-147
16. Sharma AK, Pandey AK, Kaur B (2019) Fluoride fiber-based plasmonic biosensor with two-dimensional material heterostructures: Enhancement of overall figure-of-merit via optimization of radiation damping in near infrared region. Materials 12(9):1542
17. Cordeiro CMB, Franco MAR, Chesini G, Barretto ECS, Lwin R, Brito Cruz CH, Large MCJ (2006) Microstructured-core optical fibre for evanescent sensing applications. Opt Express 14, 13056
18. Morshed M, Hassan MI, Roy TK, Uddin MS, Razzak SA (2015) Microstructure core photonic crystal fiber for gas sensing applications. Appl Opt 54:8637–8643
19. Bozolan A, Gerosa RM, de Matos CJS, Romero MA (2012) Temperature sensing using colloidal-core photonic crystal fiber. IEEE Sens J 12:195–200
20. Leon MJBM, Kabir MA (2020) Design of a liquid sensing photonic crystal fiber with high sensitivity, bireferingence & low confinement loss. Sens Bio-Sens Res 28:100335
21. Pinto AMR, Lopez-Amo M (2012) Photonic crystal fibers for sensing applications. J Sens 2012:598178
22. Ma M et al (2019) Highly sensitive temperature sensor based on Sagnac interferometer with liquid crystal photonic crystal fibers. Optik (Stuttg) 179:665–671
23. Hameed MFO, Obayya SSA, Computational Photonic Sensors, Springer, 2018 June.
24. Tong K, Wang F, Wang M, Dang P, Wang Y, Sun J (2018) D-shaped photonic crystal fiber biosensor based on silver-graphene. Optik (Stuttg) 168:467–474
25. Azab MY, Hameed MFO, Obayya SSA (2019). Multifunctional Plasmonic Photonic Crystal Fiber Biosensors. https://doi.org/10.1007/978-3-319-76556-3_10
26. Pinto AMR, Lopez-Amo M (2012) Photonic crystal fibers for sensing applications. J Sens 598178
27. Jain RK, Cui ZC, Domen JK (2016) Environmental impacts of mining. Environmental impact of mining and mineral processing: 53–157
28. Miller BG (2017) The effect of coal usage on human health and the environment. Clean Coal Engineering Technology: 105–144
29. Leon, Md Jayed Bin Murshed, and Md Ahasan Kabir (2020) Design of a liquid sensing photonic crystal fiber with high sensitivity, bireferingence & low confinement loss." Sensing and Bio-Sensing Research 28: 100335
30. Zhang, Yani, et al. "Porous photonic-crystal fiber with near-zero ultra-flattened dispersion and high birefringence for polarization-maintaining terahertz transmission." Optik 207 (2020): 163817.
31. Eid, Mahmoud MA, et al. "Highly sensitive nonlinear photonic crystal fiber based sensor for chemical sensing applications." *Microsystem Technologies* 27.3 (2021): 1007–1014.
32. Eid MMA, Habib MA, Anower MS, Rashed ANZ (2020) Highly sensitive nonlinear photonic crystal fiber based sensor for chemical sensing applications. Microsyst Technol. 1–8
33. Nyachionjeka K, Tarus H, Langat K (2020) Design of a Photonic Crystal Fiber for Optical Communications Application, Scientific African
34. Ayyanar N, Raja RV, Vigneswaran D, Lakshmi B, Sumathi M, Porsezian K (2017) Highly efficient compact temperature sensor using liquid infiltrated asymmetric dual elliptical core photonic crystal fiber. Opt Mater 64:574–582

35. Agrawal GP (2001) Nonlinear Fiber Optics. Academic Press, San Diego
36. Sardar, Md Ranju, and Mohammad Faisal. Methane gas sensor based on microstructured highly sensitive hybrid porous core photonic crystal fiber. Journal of Sensor Technology 9.1 (2019): 12–26.
37. Rabee, Ahmed Saber H., et al. Highly sensitive photonic crystal fiber gas sensor. Optik 188 (2019): 78–86.
38. Paul, Bikash Kumar, et al. Investigation of gas sensor based on differential optical absorption spectroscopy using photonic crystal fiber. Alexandria Engineering Journal 59.6 (2020): 5045–5052.
39. Abbaszadeh A, Makouei S, Meshgini S (2021) High sensitive triangular photonic crystal fiber sensor design applicable for gas detection. Advanced Electromagnetics 10(1):1–5
40. Nizar, S. Mohamed, Elizabeth Caroline, and Prabu Krishnan. Design and investigation of a high-sensitivity PCF sensor for the detection of sulfur dioxide. Plasmonics (2021): 1–11.
41. Leon, Md Jayed Bin Murshed, and Asma Safia Disha. A simple structure of PCF based sensor for sensing sulfur dioxide gas with high sensitivity and better birefringence. Sensors International (2021): 100115.
42. Abbaszadeh A, Makouei S, Meshgini S (2022) New hybrid photonic crystal fiber gas sensor with high sensitivity for ammonia gas detection. Can J Phys 100(2):129–137